LETTER

Light D-wave axial-tensor $K_2(1820)$ meson at finite temperature

To cite this article: A. Türkan *et al* 2019 *EPL* **126** 51001

epl A Letters Journal Exploring the Frontiers of Physics

June 2019

EPL, **126** (2019) 51001 www.epljournal.org
doi: 10.1209/0295-5075/126/51001

Light D-wave axial-tensor $K_2(1820)$ meson at finite temperature

A. Türkan[1], H. Dağ[2], J. Y. Süngü[3] and E. Veli Veliev[3]

[1] *Özyeğin University, Department of Natural and Mathematical Sciences - Çekmeköy, Istanbul, Turkey*
[2] *Physik Department, Technische Universität München - D-85747 Garching, Germany*
[3] *Department of Physics, Kocaeli University - 41380 Izmit, Turkey*

received 17 February 2019; accepted in final form 11 June 2019
published online 9 July 2019

PACS 11.55.Hx – Sum rules
PACS 14.40.-n – Mesons
PACS 11.10.Wx – Finite-temperature field theory

Abstract – In this work the properties of the axial-tensor $K_2(1820)$ meson in a hot medium are investigated. The mass and the decay constant of this state are calculated via thermal QCD sum rules considering QCD condensates up to dimension five. Our analysis show that both mass and decay constant stay almost monotonous up to certain temperatures and then they diminish with increasing temperature. The mass and decay constant estimated at zero temperature are in good agreement with the present experimental data and theoretical estimations.

Introduction. – The features of hadronic matter under extreme densities and temperatures such as deconfinement of quarks and gluons creating strongly interacting Quark-Gluon-Plasma (QGP) are significant topics of high-energy physics within last decades [1–5]. After being predicted by Matsui and Satz in ref. [2], the suppression of the J/ψ state in hot medium was considered as a signature for the QGP production in heavy-ion collision experiments [6–9]. In this context, numerous studies have been devoted to the determination of the thermal properties of hadrons in a hot medium [10–20]. Studying thermal properties of hadrons and their fate in high temperatures gives us an understanding about the collective behavior of strongly interacting matter and it also helps us to explore the mechanisms behind confinement and chiral symmetry breaking. The critical temperature, at which QCD phase transition occurs in QGP and hadronic matter, is estimated as $T_c \cong 155\,\text{MeV}$ by Andronic, Braun-Munzinger *et al.* [21], analyzing the experimental data from heavy ion collisions at RHIC and LHC via theoretical efforts [22,23] while Beccattini *et al.* supposed that deconfinement temperature should be between 160 and 165 MeV [24] using the UrQMD hybrid model. Lattice QCD also predicted a transition temperature from partonic stage to hadronic matter with a smooth crossover [4,25–29]. In general, the decay constants and the masses of physical states are estimated to decrease with increasing temperature, while hadronic widths of these states increase [5,10].

Studying tensor mesons is relatively more complicated when compared with scalars or vectors. The classification of these states into the $q\bar{q}$ scenario is an alluring question, since the number of the observed states are more than those required by the Quark Model (QM). Tensor mesons with $J^{PC} = 2^{++}$ are examples of a very well-known $q\bar{q}$ nonet, and their decays match nicely into this scheme [30,31]. However, the chiral partners of tensor mesons, the axial-tensor mesons (1^3D_2, $I(J^{PC}) = 2^{--}$), are not so well understood including $K_2(1820)$ [32–34]. Axial-tensor systems were investigated by theoretical models such as the quadratic spinless Salpeter-type equation (QSSTE) [35], the non-relativistic quark model (NRQM) with instanton-induced interaction [36], the Godfrey-Isgur model (GIM) and its modifications [30,31], the relativistic quark model (RQM) [37] and QCD sum rules (QCDSR) [38].

In this work we concentrated on the mass and the decay constant of the ground-state $[d\bar{s}]$ axial-tensor meson $K_2(1820)$. We used thermal QCD sum rules including the quark, gluon and mixed condensates corrections up to dimension five. We modified the quark-hadron duality with a temperature-dependent threshold and replaced the vacuum expectation values of condensates with thermal forms. This article is organized as follows. In the following section we present the formalism of thermal QCD sum rules for $K_2(1820)$. In the third section, we give our numerical analysis to estimate the mass and the decay constant of $K_2(1820)$ at vacuum and also at finite

temperatures. Results and discussions are presented at the end of the third section.

Thermal QCD sum rules for $K_2(1820)$. – The sum rules to obtain the mass and the decay constant of the axial-tensor meson are derived from the following two-point thermal correlation function:

$$\Pi_{\mu\nu,\alpha\beta}(q,T) = i\int \mathrm{d}^4x e^{iq\cdot(x-y)} \times \mathrm{Tr}\{\rho\mathcal{T}[J_{\mu\nu}(x)J^{\dagger}_{\alpha\beta}(y)]\}_{|y\to 0}, \quad (1)$$

where $J_{\mu\nu}$ is the interpolating current of $K_2(1820)$. In eq. (1), $\rho = e^{-H/T}/Tr(e^{-H/T})$ is the thermal density matrix, T is the temperature, H is the QCD Hamiltonian and $\mathcal{T}$ is the time-ordered product. The interpolating current is chosen as [38]

$$J_{\mu\nu}(x) = \frac{i}{2}\big[\bar{s}(x)\gamma_\mu\gamma_5 \overleftrightarrow{\mathcal{D}}_\nu\,(x)d(x) + \bar{s}(x)\gamma_\nu\gamma_5 \overleftrightarrow{\mathcal{D}}_\mu\,(x)d(x)\big], \quad (2)$$

where $\overleftrightarrow{\mathcal{D}}_\mu\,(x) = \frac{1}{2}[\overrightarrow{\mathcal{D}}_\mu\,(x) - \overleftarrow{\mathcal{D}}_\mu\,(x)]$, $\lambda^a (a = 1,8)$ and $A^a_\mu(x)$ are the Gell-Mann matrices and gluon fields, respectively. In thermal QCD sum rules, similar to vacuum sum rules [39] the dual nature of the correlation function given in eq. (1) is used to extract information on the medium properties of hadrons. At large distances, the correlation function is expressed in terms of hadronic parameters, such as mass and decay constant, which is referred as the physical side. While at short distances, the correlation function is expressed in terms of QCD parameters such as quark masses, quark condensates, and calculation of the correlation function in these regions is often called as the QCD side. The basic idea of the QCD sum rules method is to calculate the correlation function in both regions, and then there should be a q^2 region in which both expressions can be equated to extract physical features of hadrons.

To obtain the correlation function from the physical side, a complete set of intermediate physical states are inserted into eq. (1), and related integrals over four-x are performed. Hence, finally the correlation function is obtained in terms of matrix elements of the hadronic states as

$$\Pi^{phys}_{\mu\nu,\alpha\beta}(q,T) = \frac{\langle\omega \mid J_{\mu\nu}(0) \mid K_2\rangle\langle K_2 \mid \bar{J}_{\alpha\beta}(0) \mid \omega\rangle}{m^2_{K_2}(T) - q^2} + \cdots, \quad (3)$$

where ω represents the hot medium state and dots indicate the contributions coming from the higher states and continuum. The matrix element $\langle\omega \mid J_{\mu\nu}(0) \mid K_2\rangle$ is defined in terms of the decay constant $f_{K_2}(T)$ and the mass $m_{K_2}(T)$ as

$$\langle\omega \mid J_{\mu\nu}(0) \mid K_2\rangle = f_{K_2}(T)m^3_{K_2}(T)\varepsilon_{\mu\nu}, \quad (4)$$

where $\varepsilon_{\mu\nu}$ is the polarization tensor satisfying the following equalities:

$$\varepsilon_{\mu\nu}\varepsilon^*_{\alpha\beta} = \frac{1}{2}\eta_{\mu\alpha}\eta_{\nu\beta} + \frac{1}{2}\eta_{\mu\beta}\eta_{\nu\alpha} - \frac{1}{3}\eta_{\mu\nu}\eta_{\alpha\beta}, \quad (5)$$

$$\eta_{\mu\nu} = -g_{\mu\nu} + \frac{q_\mu q_\nu}{m^2_{K_2}}. \quad (6)$$

Inserting eqs. (4), (5) and (6) into eq. (3), the final expression of the correlation function from the physical side is obtained as

$$\Pi^{phys}_{\mu\nu,\alpha\beta}(q,T) = \frac{f^2_{K_2}(T)m^6_{K_2}(T)}{m^2_{K_2}(T) - q^2}\left\{\frac{1}{2}(g_{\mu\alpha}g_{\nu\beta} + g_{\mu\beta}g_{\nu\alpha})\right\} + \text{other structures} + \cdots, \quad (7)$$

where only the Lorentz structures of interest are shown explicitly.

On the QCD approach, the correlation function given in eq. (1) is also expanded in terms of selected Lorentz structures as

$$\Pi^{\mathrm{QCD}}_{\mu\nu,\alpha\beta}(q,T) = \Pi^{\mathrm{QCD}}(q,T)\left\{\frac{1}{2}(g_{\mu\alpha}g_{\nu\beta} + g_{\mu\beta}g_{\nu\alpha})\right\} + \text{other structures}, \quad (8)$$

and then separated considering short-distance and long-distance effects as

$$\Pi^{\mathrm{QCD}}(q,T) = \Gamma(q,T) + \Gamma'(q,T), \quad (9)$$

where $\Gamma(q,T)$ denotes the perturbative contributions and $\Gamma'(q,T)$ denotes the non-perturbative contributions to the coefficient of structure $\frac{1}{2}(g_{\mu\alpha}g_{\nu\beta} + g_{\mu\beta}g_{\nu\alpha})$. In the QCD side, the short-distance contributions are calculated by using the perturbation theory, and written in terms of a dispersion relation as

$$\Gamma(q,T) = \int \mathrm{d}s\frac{\rho(s)}{s - q^2}, \quad (10)$$

where $\rho(s)$ is the spectral density,

$$\rho(s) = \frac{1}{\pi}Im[\Gamma(s,T)]. \quad (11)$$

On the other hand, the non-perturbative contributions to the correlation function have to be represented in terms of thermal expectation values of the quark and gluon condensates, and the thermal average of the energy density. In order to calculate all contributions coming from the QCD side, the explicit form of the interpolating current in eq. (2) is inserted into eq. (1). After standard manipulations, the QCD side of the correlation function yields

$$\Pi^{\mathrm{QCD}}_{\mu\nu,\alpha\beta}(q,T) = \frac{i}{16}\int \mathrm{d}^4x e^{iq\cdot x} \times\Bigg\{Tr\Big[S_s(y-x)\gamma_\mu\gamma_5 \overleftrightarrow{\mathcal{D}}_\nu\,(x) \overleftrightarrow{\mathcal{D}}_\beta\,(y)S_d(x-y)\gamma_\alpha\gamma_5\Big] + [\beta\leftrightarrow\alpha] + [\nu\leftrightarrow\mu] + [\beta\leftrightarrow\alpha,\nu\leftrightarrow\mu]\Bigg\}\Bigg|_{y\to 0}, \quad (12)$$

where $S_q(x-y)$ is the thermal light quark propagator in coordinate space, and it is given as

$$S_q^{ij}(x-y) = i\frac{\not{x}-\not{y}}{2\pi^2(x-y)^4}\delta_{ij} - \frac{m_q}{4\pi^2(x-y)^2}\delta_{ij} - \frac{\langle\bar{q}q\rangle_T}{12}\delta_{ij} - \frac{(x-y)^2}{192}m_0^2\langle\bar{q}q\rangle_T\Big[1 - i\frac{m_q}{6}(\not{x}-\not{y})\Big]\delta_{ij} + \frac{i}{3}\Big[(\not{x}-\not{y})\Big(\frac{m_q}{16}\langle\bar{q}q\rangle_T - \frac{1}{12}\langle u^\mu\Theta^f_{\mu\nu}u^\nu\rangle\Big) + \frac{1}{3}\Big(u\cdot(x-y)\not{u}\langle u^\mu\Theta^f_{\mu\nu}u^\nu\rangle\Big)\Big]\delta_{ij} - \frac{ig_sG_{\mu\nu}}{32\pi^2(x-y)^2} \times\Big((\not{x}-\not{y})\sigma^{\mu\nu} + \sigma^{\mu\nu}(\not{x}-\not{y})\Big)\delta_{ij}, \quad (13)$$

where u_μ and $\Theta^f_{\mu\nu}$ are, respectively, the four-velocity of the heat bath and the fermionic part of the energy momentum tensor. In the rest frame $u_\mu = (1,0,0,0)$, *i.e.*, $u^2 = 1$, the temperature-dependent quark condensates are parameterized in terms of vacuum condensates. We used the normalized thermal quark condensate in ref. [40] by fitting lattice data [41]

$$\langle\bar{q}q\rangle_T = \langle 0|\bar{q}q|0\rangle f(T). \quad (14)$$

Here

$$f(T) = (Ae^{\alpha T} + B)^{3/2}. \quad (15)$$

In eq. (15) $\alpha = 0.0412\,\mathrm{MeV}^{-1}$, $A = -6.444\times10^{-4}$, and $B = 0.994$ are coefficients of the fit function. Also the fermionic part of the energy density is parameterized as [17]

$$\langle\Theta_{00}\rangle = T^4\mathrm{exp} \times\left(113.867\left[\frac{1}{\mathrm{GeV}^2}\right]T^2 - 12.190\left[\frac{1}{\mathrm{GeV}}\right]T\right) -10.141\left[\frac{1}{\mathrm{GeV}}\right]T^5. \quad (16)$$

After calculating the correlation function on the QCD and physical sides, by equating the coefficients of structures $\{\frac{1}{2}(g_{\mu\alpha}g_{\nu\beta} + g_{\mu\beta}g_{\nu\alpha})\}$, sum rules for $K_2(1820)$ are obtained. In general, the spectral densities are parameterized as a single sharp pole representing the lowest state hadron, and then the quark hadron duality

$$\rho(s)_{continuum} = \rho^{\mathrm{QCD}}(s)\theta(s - s_0(T)) \quad (17)$$

is employed to isolate the ground state, where $\rho(s)_{continuum}$ is the spectral density of the continuum given in eq. (3) and $s_0(T)$ is the temperature-dependent continuum threshold which is related to continuum threshold at vacuum as [21]

$$\frac{s_0(T)}{s_0(0)} = \left[\frac{\langle\bar{q}q\rangle(T)}{\langle\bar{q}q\rangle(0)}\right]^{2/3}, \quad (18)$$

which follows from deconfinement, and also restoration of chiral symmetry for light quarks, at critical temperature. After this step, Borel transformation with respect to q^2 is applied to improve the matching between the physical and QCD sides of the sum rules. After these straightforward steps, the sum rules for $K_2(1820)$ are obtained as

$$f^2_{K_2}(T)m^6_{K_2}(T)e^{-m^2_{K_2}(T)/M^2} = \int_{s_{min}}^{s_0(T)}\mathrm{d}s\rho(s)e^{-s/M^2} + \hat{\mathcal{B}}\Gamma'(q,T), \quad (19)$$

where $\hat{\mathcal{B}}$ denotes the Borel transformation with respect to q^2, and M^2 is the Borel mass parameter. The sum rules for the mass are derived following eq. (19) as

$$m^2_{K_2}(T) = \frac{\int_{s_{min}}^{s_0(T)}\mathrm{d}s\rho(s)se^{-s/M^2} + \frac{\mathrm{d}}{\mathrm{d}(-1/M^2)}\hat{\mathcal{B}}\Gamma'(q,T)}{\int_{s_{min}}^{s_0(T)}\mathrm{d}s\rho(s)e^{-s/M^2} + \hat{\mathcal{B}}\Gamma'(q,T)}, \quad (20)$$

where $s_{min} = (m_d + m_s)^2$. The spectral density and the non-perturbative contributions to the correlation function are obtained as

$$\rho(s) = \frac{3s^2 - 10sm_dm_s}{80\pi^2}, \quad (21)$$

$$\Gamma'(q,T) = \frac{4\langle u\Theta^f u\rangle(q\cdot u)^2}{3q^2} + \frac{m_0^2(m_s\langle\bar{d}d\rangle_T + m_d\langle\bar{s}s\rangle_T)}{4q^2}, \quad (22)$$

where contributions of the gluon condensates are neglected, since they are very small [42].

Numerical results and discussions. – The numerical values of the input parameters in order to analyze the obtained sum rules are given in table 1. To assure the reliability of the sum rules at finite temperature, the obtained sum rules should be tested in vacuum, *i.e.*, $T = 0$. The expressions of the mass and decay constant, given in eqs. (19) and (20), depend on two parameters arising from the aforementioned discussions given in the previous section. These parameters are the continuum threshold (s_0), and the Borel mass (M^2). In general, s_0 is related to m_{K_2} via relation $(m_{K_2} + 0.3\,\mathrm{GeV})^2 \leq s_0 \leq (m_{K_2} + 0.5\,\mathrm{GeV})^2$. However, within this region, s_0 should jointly satisfy the following criteria, pole dominance and OPE convergence, together with M^2. In addition to these criteria, physical results should be stable with respect to small variations of s_0 and M^2.

In QCD sum rules, the contribution of the ground-state hadron to the correlation function should be greater than the contribution of the continuum. To analyze the pole dominance, the variation of the ratio

$$\frac{\Pi(s_0, M^2, T=0)}{\Pi(\infty, M^2, T=0)}$$

with respect to s_0 and M^2 is plotted in fig. 1, where pole dominance of 50% is achieved in the region on the left of

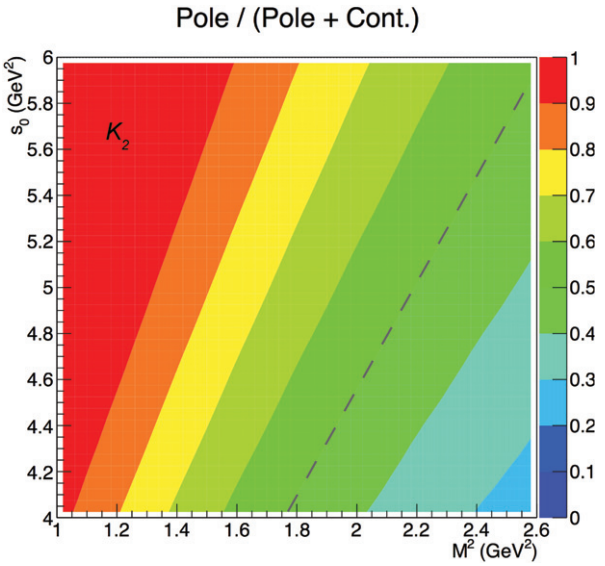

Fig. 1: The variation of the ratio of the pole to pole plus continuum with respect to s_0 and M^2 at $T = 0$ for $K_2(1820)$. Pole dominance is achieved on the left of the dashed line.

Table 1: Input parameters used in numerical analysis [43–45].

Parameters	Values
m_d	$(4.8^{+0.5}_{-0.3})$ MeV
m_s	(95.0 ± 5) MeV
m_0^2	(0.8 ± 0.2) GeV^2
$\langle 0\|\overline{u}u\|0\rangle = \langle 0\|\overline{d}d\|0\rangle$	$-(0.24 \pm 0.01)^3$ GeV^3
$\langle 0\|\overline{s}s\|0\rangle$	$-0.8(0.24 \pm 0.01)^3$ GeV^3

the dashed line. Following this discussion, we chose the working regions for s_0 and M^2 as

$$1.8\,\text{GeV}^2 \leq M^2 \leq 2.2\,\text{GeV}^2,$$
$$2.14\,M^2 + 0.24\,\text{GeV}^2 \leq s_0 \leq 5.4\,\text{GeV}^2,$$

where the lower limit of s_0 is found by applying a linear fit to the dashed line in fig. 1. In addition to pole dominance, the obtained sum rules should satisfy the convergence of OPE, which is generally characterized by the ratio of the contribution of the highest-order condensate to all contributions to correlation function, *i.e.*, the ratio $\Pi^{(D5)}/\Pi^{\text{total}}$, where $\Pi^{(D5)}$ denotes the contribution coming from operators with dimension five. In order to have reliable sum rules, the aforementioned ratio should be smaller than 20%. Within the obtained working regions, the sum rules obtained for the $K_2(1820)$ meson at $T = 0$ yield a ratio which is smaller than 5%, thus OPE convergence is also satisfied. Finally, M^2 and s_0 dependences of the mass and the decay constant at vacuum are plotted in fig. 2, where the dependences of hadronic parameters to M^2 and s_0 are observed to be weak. Thus, the obtained sum rules are reliable in predicting the mass and the decay constant, and also for exploring their thermal

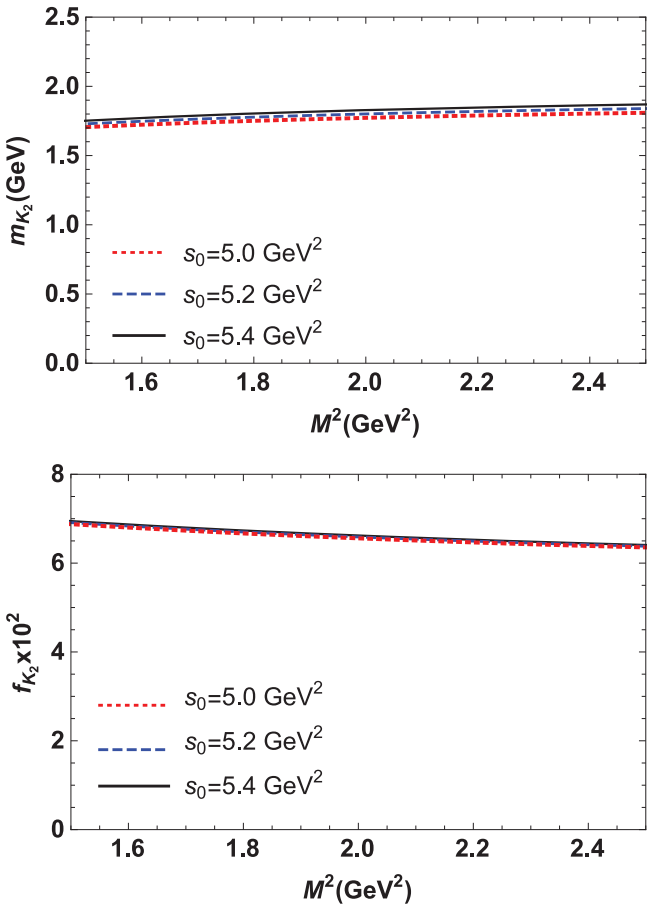

Fig. 2: Dependence of the mass (top) and the decay constant (bottom) of the axial-tensor $K_2(1820)$ meson to M^2.

Table 2: Mass and decay constant values of the axial-tensor $K_2(1820)$, obtained in this work at $T = 0$ and comparison of the findings with the other theoretical estimations and experimental results.

	Mass (MeV)	Decay constant
This Work	1800^{+47}_{-49}	$(6.59^{+0.08}_{-0.07}) \times 10^{-2}$
QSSTE [35]	1817	–
GIM [30]	1804	–
MGI [31]	1789	–
RQM [37]	1824	–
QCDSR [38]	1850 ± 140	$(6.2 \pm 0.4) \times 10^{-2}$
Experiment [43]	1819 ± 12	–

behaviors. Our estimations for the mass and the decay constant of the axial-tensor $K_2(1820)$ meson at vacuum are presented in table 2, together with corresponding uncertainties. These results are in good agreement with the ones appearing in the literature. However due to the different input parameters, our numerical results for the mass and decay constant are slightly different from ref. [37].

After obtaining reliable QCD sum rules for $K_2(1820)$ at vacuum, the analysis is extended to explore the

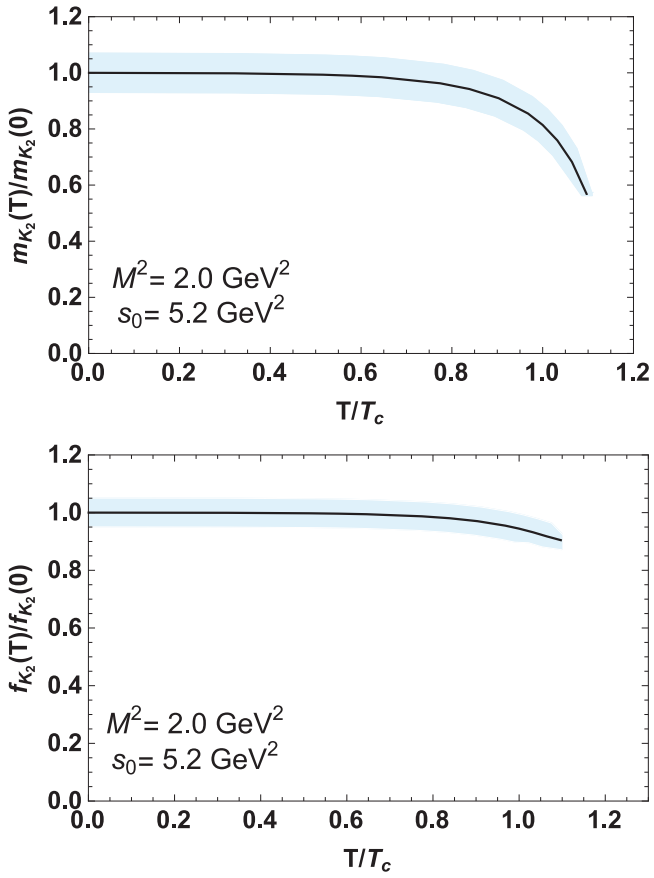

Fig. 3: The normalized thermal behavior of the mass (top) and decay constant (bottom) of the $K_2(1820)$ meson.

temperature dependence of the mass and the decay constant. Following eqs. (19) and (20), variations of the mass and the decay constant with respect to temperature are plotted in fig. 3. It is seen that the mass of $K_2(1820)$ remains unchanged until $T \cong 0.115\,\text{GeV}$ while the decay constant is stable until $T \cong 0.135\,\text{GeV}$. However after this temperature, they begin to decrease with increasing temperature. Near the critical temperature, the mass and decay constant of $K_2(1820)$ approach to 66% and 90% of their values in vacuum, respectively. These patterns show that the mass and the decay constant of the light axial-tensor $K_2(1820)$ meson dissolve at the critical temperature.

One of the most noteworthy works in the literature similar to this study is in ref. [46] where numerical calculations in Thermal QCDSR indicate that the mass of the ρ meson and its coupling with the vector current remain almost unaffected by the rise of temperature up to about 125 MeV. On the other hand, at higher temperatures the results, particularly for the mass shift of ρ meson appears unstable. Also in ref. [10] the leptonic decay constant of both pseudoscalar and vector mesons decreases with increasing T and vanishes at a critical temperature T_c. Conversely, the masses show little dependence on the temperature, except very close to T_c, where the pseudoscalar meson masses rise slightly by (10–20)%, and the vector meson masses diminish by some (20–30)%. In other works, the $D_{s0}(2317)$ meson mass decreases with increasing temperature and loses approximately (10–15)% of its mass and also the decay constant decreases with growing temperature and vanishes approximately when the critical temperature is assumed to be 150 MeV in ref. [47]. Moreover, in ref. [48] the heavy pseudoscalar mesons (B_c, η_c and η_b) masses and decay constants remain unchanged under $T \cong 100\,\text{MeV}$, but after this point, they start to decrease with increasing the temperature. At deconfinement temperature, the decay constants arrive approximately at 38% of their values in the vacuum, while the masses are decreased about 5%, 10% and 2% for B_c, η_c and η_b states, respectively. Additionally, in ref. [49] as the current coupling has fallen by half of its vacuum value for the ρ meson, mass exhibits a dramatic growth of roughly 30% near T_c, although it remains non-zero at $T = T_c$ being $T_c = 197\,\text{MeV}$. In another work, vector Υ and pseudoscalar η_b bottonium ground states are studied at finite temperature [50]. In this study, the decay width increases with rising temperature, similarly to the case of light and heavy-light-quark systems, but close to the critical temperature, T_c for $T/T_c = 0.9$ with $T_c = 200\,\text{MeV}$. The leptonic decay constant is basically a monotonically increasing function of the temperature, while their results for the thermal mass in both bottonium channels show a very slight decrease with increasing temperature.

We hope that the findings of all these studies and our results can be tested in the future, both by theoretical and experimental researches, and might help us to explore the nature of strong interactions in a hot medium.

* * *

AT, JYS and EVV acknowledge Kocaeli University for supporting through the grant BAP 2018/082. HD acknowledges support through the Scientific and Technological Research Council of Turkey (TUBITAK) BIDEP-2219 grant.

REFERENCES

[1] Bochkarev A. I. and Shaposhnikov M. E., *Nucl. Phys. B*, **268** (1986) 220.
[2] Matsui T. and Satz H., *Phys. Lett. B*, **178** (1986) 416.
[3] Hatsuda T., Koike Y. and Lee S. H., *Nucl. Phys. B*, **394** (1993) 221.
[4] Bazavov A. *et al.*, *Phys. Rev. D*, **85** (2012) 054503.
[5] Ayala A., Dominguez C. A. and Loewe M., *Adv. High Energy Phys.*, **2017** (2017) 9291623.
[6] COMPASS Collaboration, Krinner F., *EPJ Web of Conferences*, **137** (2017) 05012.
[7] ALICE Collaboration, Acharya S. *et al.*, *Phys. Rev. C*, **97** (2018) 024906.
[8] Ivanov Y. B. and Soldatov A. A., *Phys. Rev. C*, **97** (2018) 021901.

[9] Singh C. R., Ganesh S. and Mishra M., *Eur. Phys. J. C*, **79** (2019) 147.
[10] Dominguez C. A., Loewe M. and Rojas J. C., *JHEP*, **08** (2007) 040.
[11] Veliev E. V. and Aliev T. M., *J. Phys. G*, **35** (2008) 125002.
[12] Veliev E. V. and Kaya G., *Eur. Phys. J. C*, **63** (2009) 87.
[13] Mallik S. and Sarkar S., *Phys. Rev. D*, **65** (2002) 016002.
[14] Leupold S., Metag V. and Mosel U., *Int. J. Mod. Phys. E*, **19** (2010) 147.
[15] Karsch F., Kharzeev D. and Tuchin K., *Phys. Lett. B*, **663** (2008) 217.
[16] Azizi K. and Er N., *Phys. Rev. D*, **81** (2010) 096001.
[17] Azizi K. and Kaya G., *Eur. Phys. J. Plus*, **130** (2015) 172.
[18] Azizi K., Türkan A., Sundu H. and Veli Veliev E., *Adv. High Energy Phys.*, **2015** (2015) 794243.
[19] Azizi K., Sundu H., Türkan A. and Veliev E. V., *J. Phys. G*, **41** (2014) 035003.
[20] Türkan A., Dağ H., Süngü J. Y. and Veliev E. V., *EPJ Web of Conferences*, **199** (2019) 03007.
[21] Andronic A., Braun-Munzinger P., Redlich K. and Stachel J., *Nature*, **561** (2018) 7723321.
[22] HotQCD Collaboration (Steinbrecher P.), *Nucl. Phys. A*, **982** (2019) 847.
[23] Bazavov A. *et al.*, *Phys. Rev. D*, **95** (2017) 5054504.
[24] Becattini F., Bleicher M., Kollegger T., Schuster T., Steinheimer J. and Stock R., *Phys. Rev. Lett.*, **111** (2013) 082302.
[25] Rajagopal K., *Acta Phys. Pol. B*, **31** (2000) 3021.
[26] CP-PACS Collaboration (Khan A. A. *et al.*), *Phys. Rev. D*, **63** (2001) 034502.
[27] Karsch F., *Nucl. Phys. Proc. Suppl.*, **83** (2000) 14.
[28] Wuppertal-Budapest Collaboration (Borsanyi S. *et al.*), *JHEP*, **09** (2010) 073.
[29] Aoki Y., Endrodi G., Fodor Z., Katz S. D. and Szabo K. K., *Nature*, **443** (2006) 675.
[30] Godfrey S. and Isgur N., *Phys. Rev. D*, **32** (1985) 189.
[31] Pang C. Q., Wang J. Z., Liu X. and Matsuki T., *Eur. Phys. J. C*, **77** (2017) 861.
[32] Chen W., Cai Z. X. and Zhu S. L., *Nucl. Phys. B*, **887** (2014) 201.
[33] Wang B., Pang C. Q., Liu X. and Matsuki T., *Phys. Rev. D*, **91** (2015) 014025.
[34] Roca L., *Phys. Rev. D*, **84** (2011) 094006.
[35] Chen J. K., *Eur. Phys. J. C*, **78** (2018) 648.
[36] Monterio A. P. and Kumar K. B. V., *Indian J. Pure Appl. Phys.*, **48** (2010) 240.
[37] Ebert D., Faustov R. N. and Galkin V. O., *Phys. Rev. D*, **79** (2009) 114029.
[38] Aliev T. M., Bilmis S. and Yang K. C., *Nucl. Phys. B*, **931** (2018) 132.
[39] Shifman M. A., Vainshtein A. I. and Zakharov V. I., *Nucl. Phys. B*, **147** (1979) 385.
[40] Dominguez C. A. and Hernandez L. A., *Mod. Phys. Lett. A*, **31** (2016) 361630042.
[41] Bali G. S., Bruckmann F., Endrodi G., Fodor Z., Katz S. D. and Schafer A., *Phys. Rev. D*, **86** (2012) 071502.
[42] Aliev T. M. and Shifman M. A., *Phys. Lett. B*, **112** (1982) 401.
[43] Particle Data Group (Tanabashi M. *et al.*), *Phys. Rev. D*, **98** (2018) 030001.
[44] Ioffe B. L., *Prog. Part. Nucl. Phys.*, **56** (2006) 232.
[45] Narison S., *Phys. Lett. B*, **605** (2005) 319.
[46] Mallik S. and Mukherjee K., *Phys. Rev. D*, **58** (1998) 096011.
[47] Veliev E. V. and Kaya G., *Acta Phys. Pol. B*, **41** (2010) 1905.
[48] Veliev E. V., Azizi K., Sundu H. and Aksit N., *J. Phys. G*, **39** (2012) 015002.
[49] Ayala A., Dominguez C. A., Loewe M. and Zhang Y., *Phys. Rev. D*, **86** (2012) 114036.
[50] Dominguez C. A., Loewe M. and Zhang Y., *Phys. Rev. D*, **88** (2013) 054015.